FEBS Open Bio 3 (2013) 35–40

journal homepage: www.elsevier.com/locate/febsopenbio

Structure of L-rhamnose isomerase in complex with L-rhamnopyranose demonstrates the sugar-ring opening mechanism and the role of a substrate sub-binding site

Hiromi Yoshida[a], Akihide Yoshihara[b], Misa Teraoka[a], Satoshi Yamashita[a], Ken Izumori[b], Shigehiro Kamitori[a,*]

[a] Life Science Research Center and Faculty of Medicine, Kagawa University, 1750-1 Ikenobe, Miki-cho, Kita-gun, Kagawa 761-0793, Japan
[b] Rare Sugar Research Center and Faculty of Agriculture, Kagawa University, Miki-cho, Kagawa 761-0795, Japan

ARTICLE INFO

Article history:
Received 27 November 2012
Accepted 30 November 2012

Keywords:
L-Rhamnose isomerase
Pseudomonas stutzeri
Sugar-ring opening mechanism
Rare sugar
X-ray structure

ABSTRACT

L-Rhamnose isomerase (L-RhI) catalyzes the reversible isomerization of L-rhamnose to L-rhamnulose. Previously determined X-ray structures of L-RhI showed a hydride-shift mechanism for the isomerization of substrates in a linear form, but the mechanism for opening of the sugar-ring is still unclear. To elucidate this mechanism, we determined X-ray structures of a mutant L-RhI in complex with L-rhamnopyranose and D-allopyranose. Results suggest that a catalytic water molecule, which acts as an acid/base catalyst in the isomerization reaction, is likely to be involved in pyranose-ring opening, and that a newly found substrate sub-binding site in the vicinity of the catalytic site may recognize different anomers of substrates.

1. Introduction

L-Rhamnose isomerase (L-RhI), which catalyzes the reversible isomerization of L-rhamnose to L-rhamnulose (Fig. 1A), is involved in metabolism in *Escherichia coli* (*E. coli*) [1]. L-RhIs from *Lactobacillus plantarum* [2], *Arthrobacter pyridinolis* [3], *Salmonella typhimurium* [4], *Pseudomonas stutzeri* (*P. stutzeri*) [5–7], *Mesorhizobium loti* [8], *Bacillus pallidus* [9], *Bacillus halodurans* [10], *Thermotoga maritima* [11], *Thermoanaerobacterium saccharolyticu* [12], and *Caldicellulosiruptor saccharolyticus* [13] have also been characterized. Since some L-RhIs are capable of the isomerization of rare sugars, for example, between D-allose (Fig. 1B) and D-psicose, they have been attracting a lot of attention regarding the industrial production of rare sugars.

The X-ray structures of L-RhIs from *E. coli* [14] and *P. stutzeri* [15–17] have been reported previously. L-RhI forms a homo tetramer, with two adjacent metal ions at the catalytic site of each subunit. So far, two mechanisms, the ene-diol mechanism [18,19] and hydride-shift mechanism [20,21], have been proposed for aldose–ketose isomerization. The X-ray structures of L-RhIs showed that they adopt a metal-mediated hydride-shift mechanism with the transfer of a proton between O1 and O2 by a catalytic water molecule, which binds to a metal ion to be activated as a hydroxide ion (Fig. 1A) [21,22], because no amino acid residues act as an acid/base catalyst to transfer a proton between C2 and C1 for the ene-diol mechanism [14–16].

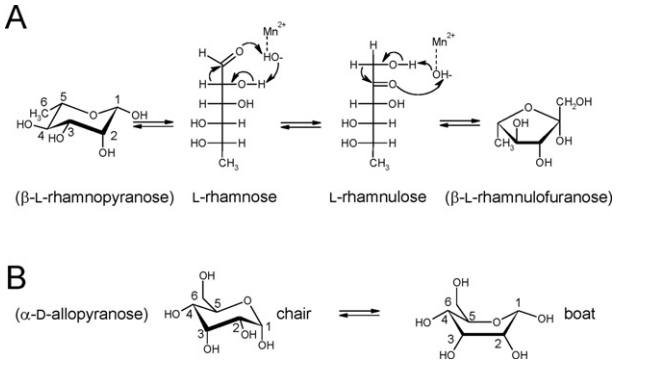

Fig. 1. Chemical reaction catalyzed by *P. stutzeri* L-RhI and chemical structure of D-allopyranose. (A) Proposed metal-mediated hydride-shift mechanism for aldose–ketose isomerization is shown with sugar-ring forms of L-rhamnose. (B) The chair and boat conformations of D-allopyranose are shown.

Abbreviations: L-RhI, L-rhamnose isomerase; *E. coli*, *Escherichia coli*; *P. stutzeri*, *Pseudomonas stutzeri*; D327N, mutant *P. stutzeri*L-RhI, with a substitution of Asp327 with Asn; H101N, mutant *P. stutzeri*L-RhI, with a substitution of H101 with Asn; RNS, L-rhamnose in a linear form; β-RPS, β-L-rhamnopyranose; α-RPS, α-L-rhamnopyranose; α-APS, α-D-allopyranose

* Corresponding author. Tel./fax: +81 87 891 2421.
E-mail address: kamitori@med.kagawa-u.ac.jp (S. Kamitori).

2211-5463
http://dx.doi.org/10.1016/j.fob.2012.11.008

We previously reported the catalytic reaction mechanism of *P. stutzeri* L-RhI, based on the X-ray structures of mutant forms in complexes with substrates. Our finding that Trp179 helps a hydride ion to shift between C1 and C2 by shielding it from the solvent strongly supported the hydride-shift mechanism [15]. Also, we successfully determined the X-ray structure of an inactive mutant *P. stutzeri* L-RhI with a substitution of Asp327 with Asn (D327N), in which substrates in a furanose-ring form (L-rhamnulofranose) bound to the catalytic site, suggesting that Asp327 is responsible for furanose-ring opening [16]. However, the pyranose-ring opening mechanism for L-rhamnopyranose remained unclear.

Fenn et al. reported the X-ray structure of *Streptomyces olivochromogenes* D-xylose isomerase, which has structural homology to *P. stutzeri* L-RhI (Supplemental Fig. S1), and proposed that a pair of adjacent residues His53 and Asp56 was responsible for pyranose-ring opening [21]. There is no corresponding pair of His and Asp residues in *P. stutzeri* L-RhI, only a His residue (His101). However, His101 forms a hydrogen bond with the O5 of a substrate, as His53 of *S. olivochromogenes* D-xylose isomerase does (Supplemental Fig. S1B), and is expected to be involved in pyranose-ring opening. Here we report the X-ray structures of a mutant *P. stutzeri* L-RhI with a substitution of His101 with Asn (H101N) in complexes with L-rhamnose and D-allose, in which substrates at the catalytic site were partly in a pyranose-ring form. In addition, a newly found substrate sub-binding site in the vicinity of the catalytic site was reported.

2. Materials and methods

2.1. Protein preparation and crystallization

For the construction of H101N, site-directed mutagenesis was carried out using a plasmid, pOI-02, encoding the L-RhI gene [7] and the Quick change Kit (Stratagene). The oligonucleotides used were forward primer 5′-CCA ATG TCT CGC TGA ACA TTC CGT GGG AC-3′ and reverse primer 5′-GTC CCA CGG AAT GTT CAG CGA GAC ATT GG-3′. H101N was purified as reported previously [15].

Purified H101N was dialyzed against a buffer solution (5 mM Tris–HCl, and 5 mM EDTA, pH 8.0) to remove bound metal ions retained from the culture medium, and the buffer was then replaced with 5 mM HEPES pH 8.0. The enzyme solution was concentrated to 8.4 mg/ml with a Microcon YM-10 filter (Millipore, Billerica, MA). H101N crystals were grown by the vapor diffusion method using a protein solution (8.4 mg/ml) and reservoir solution (7–8% (w/v) polyethylene glycol 20,000 and 50 mM MES buffer (pH 6.3)). After appropriate sized crystals were obtained, $MnCl_2$ (final concentration of 1 mM) was added to the crystallization drops. Crystals of complexes with substrates were obtained by a quick soaking method, using a solution containing 33% (w/v) L-rhamnose or D-allose as a cryoprotectant.

2.2. Data collection and structural determination

Crystals were flash-cooled in liquid nitrogen at 100 K and X-ray diffraction data were collected on PF-AR NE3A and NW12A beam lines in the Photon Factory (Tsukuba, Japan), and the BL26B1 beam line in SPring-8. Diffraction data were processed using the program HKL2000 [23] and CCP4 program suite [24]. Data collection statistics and scaling results are listed in Table 1. Initial phases were determined by a molecular replacement method with the program MOLREP [25] in the CCP4 program suite, using the structure of the wild-type *P. stutzeri* L-RhI (PDB code 2HCV) as a probe model [15]. Further model building was performed with the programs Coot [26], in the CCP4 program suite, and X-fit [27], in the XtalView program system [28], and the structure was refined using the programs Refmac5 [29] and CNS [30]. Water molecules were gradually introduced if peaks above 3.5σ in the ($F_o - F_c$) electron density map were in the range of a hydrogen bond. The number of residues in the most favored regions of a Ramachandran plot [31] was determined by the program PROCHECK [32]. Refinement statistics are listed in Table 1. Figs. 2–4 were illustrated by the program PyMol [33].

Table 1
Data collection and refinement statistics.

	H101N with -rhamnose	H101N with D-allose
Data collection		
Beamline	PF-AR NE3A	PF-AR NW12A
Temperature (K)	100	100
Wavelength (Å)	1.0	1.0
Resolution range (Å)	50.0–1.70 (1.73–1.70)	50.0–2.38 (2.42–2.38)
No. of measured refs.	639,820	195,850
No. of unique refs.	182,769 (9074)	62,445 (3085)
Redundancy	3.5 (3.4)	3.1 (2.8)
Completeness (%)	98.2 (97.8)	92.3 (91.1)
Mean $I_o/\sigma(I_o)$	11.7 (3.9)	8.3 (3.0)
R_{merge} * (%)	9.1 (32.1)	11.4 (36.4)
Space group	$P2_1$	$P2_1$
Unit cell parameters (Å)	$a = 75.1$ $b = 104.9$ $c = 112.4$ $\beta = 106.0^\circ$	$a = 74.7$ $b = 104.4$ $c = 114.0$ $\beta = 107.9^\circ$
Refinement		
Resolution range (Å)	31.48–1.70 (1.81–1.70)	37.60–2.38 (2.53–2.38)
No. of refs.	173,095 (24,342)	54,816 (7202)
Completeness (%)	94.2 (88.4)	82.1 (72.1)
R_{factor} (%)	17.7 (22.4)	20.2 (27.4)
R_{free} (%)	19.5 (25.6)	24.9 (36.0)
RMSD bond lengths (Å)	0.005	0.006
RMSD bond angles (°)	1.2	1.2
Ramachandran plot		
Most favoured region (%)	90.5	89.9
Additional allowed region (%)	9.0	9.6
B -factor ($Å^2$)		
Protein	19.0	29.9
Ligand	29.4	40.8
Solvent	30.5	23.7
PDB code	4GJI	4GJJ

Values in parentheses are of the high-resolution bin.
* $R_{merge} = \Sigma_h \Sigma_i [|I_i(h) - \langle I(h)\rangle|/\Sigma_h \Sigma_i I_i(h)]$, where I_i is the ith measurement and $\langle I(h)\rangle$ is the weighted mean of all measurements of $I(h)$.

2.3. Determination of kinetic parameters

The kinetic parameters of enzymes were determined by a cystein–carbazole assay detecting the amount of ketose produced using a calorimetric method. The reaction was initiated by the addition of various concentrations of each substrate (final concentrations of 1, 2, 5, 10, 20, 50, or 100 mM) and terminated by the addition of 50 μl of 10% trichloroacetic acid after the mixture was incubated for 10 min at 50 °C [6,17,34]. Kinetic parameters are listed in Supplemental Table S1.

3. Results

3.1. Overall structure of mutant P. stutzeri L-RhI (H101N)

The overall structure of the mutant *P. stutzeri* L-RhI (H101N) in a complex with a substrate (L-rhamnose or D-allose) was almost the same as that of wild-type *P. stutzeri* L-RhI, which has already been reported [15]. Briefly, H101N comprised a large domain with a $(\beta/\alpha)_8$ barrel fold and an additional small domain with a bundle of α-helices, and two metal ions (Mn^{2+}) bound to the center of the barrel

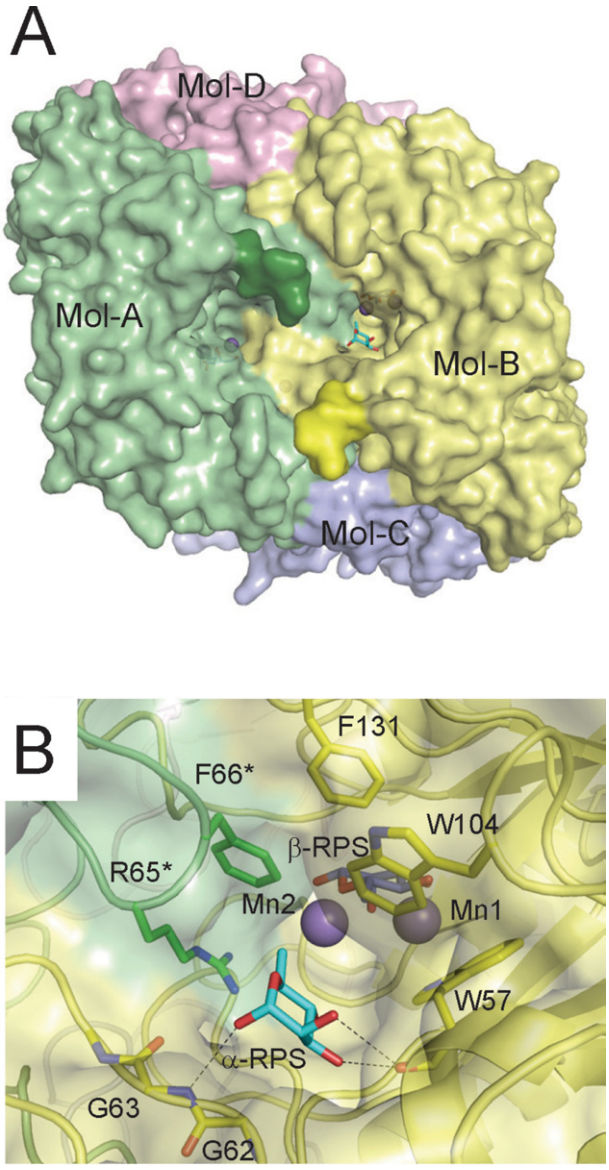

Fig. 2. Homo-tetramer structure of *P. stutzeri* L-Rhl. (A) The substrate-accessible surface of Mol-A/Mol-B is shown with bound metal ions (purple), β-RPS (blue), and α-RPS (cyan). Mol-A, Mol-B, Mol-C, and Mol-D are in yellow, green, blue, and magenta, respectively. C-terminal regions are in dark colors. (B) A close-up view of the sub-binding site of Mol-B. Amino acid residues interacting with α-RPS are shown in a stick model with hydrogen bonds (dotted lines). (For interpretation of the references to color in this figure legend, the reader is referred to the web version of this article.)

to form the catalytic site (Supplemental Fig. S2A). The enzyme formed a homo-tetramer with a 2 2 2 symmetry, composed of four molecules (Mol-A, Mol-B, Mol-C, and Mol-D). The pairs Mol-A/Mol-B and Mol-C/Mol-D formed an accessible surface for substrate-binding, on opposite sides to each other (Fig. 2A and Supplemental Fig. S2B). Substrates bound to the catalytic sites of four molecules. In the H101N/L-rhamnose complex, apart from the bound substrate in the catalytic site, bound L-rhamnopyranose was found at the entrance to the catalytic sites of Mol-B and Mol-C. This site was located at the bottom of the deep cleft of an accessible surface for substrate-binding, and was expected to act as a substrate sub-binding site (Fig. 2B and Supplemental Fig. S2B).

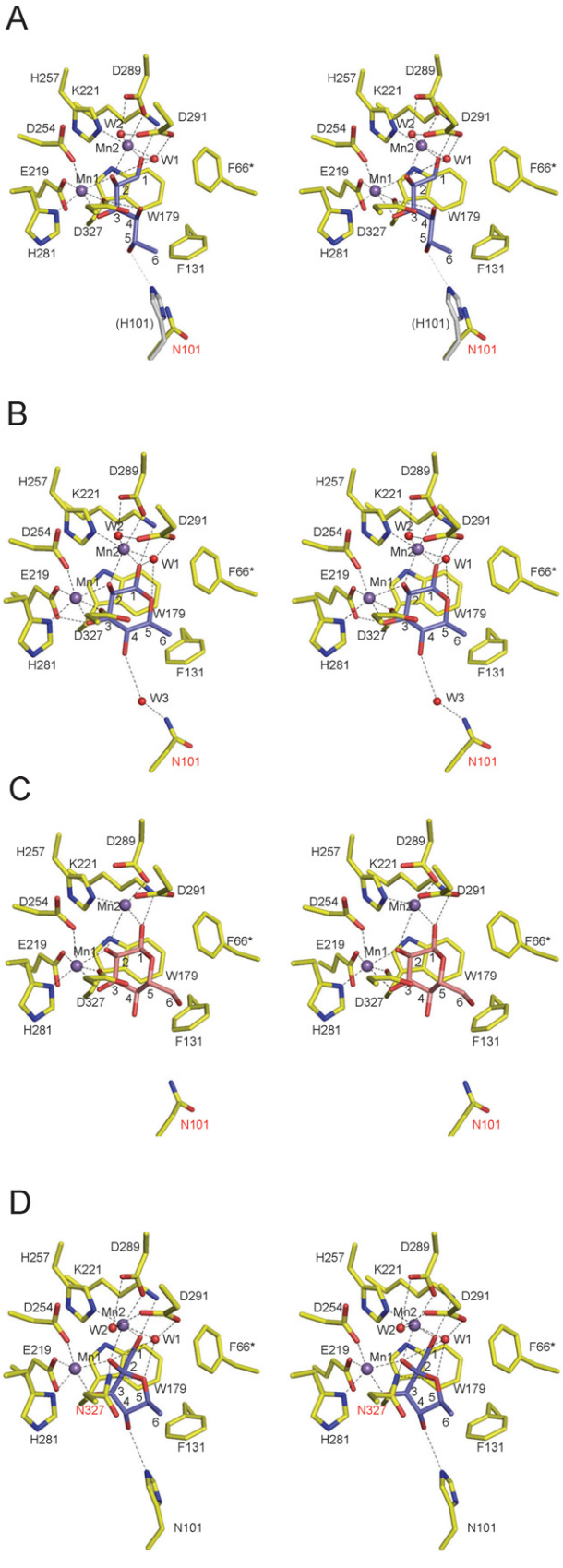

Fig. 3. Stereoview of the catalytic site with bound substrates. (A) RNS (blue) in Mol-A, (B) β-RPS (blue) in Mol-B, (C) α-APS (salmon pink) in Mol-B, and (D) β-RFS (blue) in Mol-A (PDB code 3ITL) are shown with selected interactions among amino acid residues, substrates, metal ions, and water molecules by dotted lines. Substituted amino acid resides are labeled in red, and the inherent His101 is superimposed in (A). (For interpretation of the references to color in this figure legend, the reader is referred to the web version of this article.)

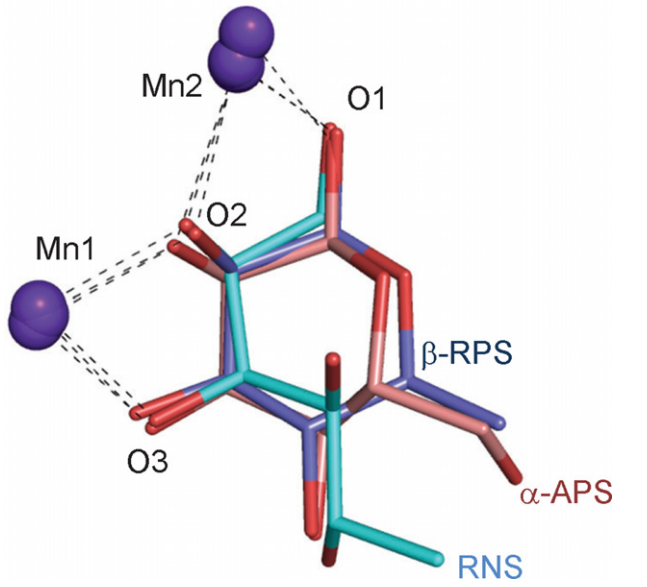

Fig. 4. Superimposed bound RNS (cyan), β-RPS (blue), and α-APS (salmon pink). (For interpretation of the references to color in this figure legend, the reader is referred to the web version of this article.)

3.2. Interactions between proteins and substrates

In the H101N/L-rhamnose complex, bound substrates at the catalytic site were found to be in a linear form in Mol-A and Mol-C, while these bound substrates adopted two alternative conformations, a linear form and pyranose-ring form, with the same occupancy of 0.5 in Mol-B and Mol-D (Supplemental Fig. S3A). The lower enzymatic activity (*Vmax* or *kcat*) of H101N (51% of the wild-type level) (Supplemental Table 1) and quick soaking using a highly concentrated substrate solution may have partially given the complex structure including a substrate in a pyranose-ring form. Since the protein–substrate interactions found in Mol-A/Mol-B were almost equivalent to those in Mol-C/Mol-D, the structural description here concentrates on the catalytic sites of Mol-A and Mol-B, and the sub-binding site of Mol-B.

The catalytic site structure with a bound L-rhamnose in a linear form (RNS) in Mol-A is shown in Fig. 3A, and was very similar to previously reported structures [15,16]. Structural Mn^{2+} (Mn1) was coordinated by six coordination bonds from Glu219(OE), Asp254(OD), His281(ND), Asp327(OD), and the O2/O3 of RNS, and catalytic Mn^{2+} (Mn2) was coordinated by His257(NE), Asp289(OD1), two water molecules (W1 and W2), and the O1/O2 of RNS. W1 was the catalytic water molecule responsible for the proton transfer between O1 and O2 (Fig. 1A). On the opposite side to W1, Phe131, Trp179, and Phe66* (Mol-B) created a hydrophobic environment favorable for the hydride-shift between C1 and C2, by shielding them from the solvent. Lys221 and Asp327 formed hydrogen bonds with RNS, fixing the substrate in the proper orientation and position. In the wild-type enzyme, His101 also formed a hydrogen bond with RNS (shown in gray in Fig. 3A).

The catalytic site structure with a bound β-L-rhamnopyranose (β-RPS) in Mol-B is shown in Fig. 3B. The conformation of C1–C3 of β-RPS was almost equivalent to that of RNS, giving the same metal-coordination structure as Mol-A. A difference was found between β-RPS and RNS for the torsion angle of C3–C4, −52° (β-RPS) and 171° (RNS), meaning that rotation around C3–C4 by +223° (or −137°) gave the inter-conversion between β-RPS and RNS. The catalytic water molecule (W1) formed a hydrogen bond with the O1 and O5 of β-RPS, likely acting as an acid/base catalyst in pyranose-ring opening. The substituted Asn101 formed a hydrogen bond with the O4 of β-RPS via a water molecule (W3), which contributed to the stabilization of the enzyme/β-RPS complex.

Bound α-L-rhamnopyranose (α-RPS) molecules were found at the sub-binding sites of Mol-B and Mol-C, a distance of 8 Å from bound substrates at catalytic sites (Fig. 2B). α-RPS approached the deep hydrophobic pocket created by Gly62, Trp57, Trp104, Phe131, Arg65*, and Phe66*, from the methyl group (C6) on the head, and formed three hydrogen bonds with the protein, namely O1 – Gly63(N), O2 – Trp57(O), and O3 – Trp57(O). The sub-binding site of Mol-D without bound α-RPS was occupied by the C-terminal region (Ala421–Ile429) of the neighboring Mol-C (Supplemental Fig. S2B). Although the C-terminal 5–8 amino acid residues of Mol-A, Mol-B, and Mol-C were invisible on the electron density map, the C-terminal residues of Mol-B and Mol-D were directed toward the outside of the sub-binding site, allowing a substrate to approach, while those of Mol-A were directed toward the sub-binding site, perhaps inhibiting the approaching of a substrate.

In the H101N/D-allose complex, the bound substrate in a pyranose-ring form was found only in Mol-B, as shown in Fig. 3C. Substrates bound to other catalytic sites were in a linear form, and there was no D-allopyranose at sub-binding sites. The electron density map showed that the bound α-APS had the boat conformation of the pyranose-ring (Supplemental Fig. S3B). The bound α-APS in the boat form superimposed well to the bound RNS and β-RPS, as shown in Fig. 4, with mean deviations of metal ions and three oxygen atoms with metal-coordination (M1, M2, O1, O2, and O3) being 0.28 Å (RNS) and 0.29 Å (β-RPS). Water molecules at the catalytic site (W1, W2, and W3) could not be found, maybe due to low resolution (2.38 Å).

4. Discussion

The previously determined structure of a mutant *P. stutzeri* L-RhI (D327N) in a complex with a 5-membered ring, β-L-rhamunulofranose (β-RFS), is shown in Fig. 3D (PDB code 3ITL). The furanose-ring had a similar orientation to the pyranose-ring, but the O5 of β-RPS moved 0.45 Å from Asp327 relative to β-RFS, suggesting that Asp327 is unlikely to protonate the O5 of β-RPS for ring-opening. The presented structure strongly suggested that a catalytic water molecule (W1) protonates O5 with a distance of 3.2 Å, and deprotonates O1 (2.8 Å) in pyranose-ring opening. The substituted Asn101 helped to stabilize the enzyme/β-RPS complex by forming a water-mediated hydrogen bond with the O4 of β-RPS, and the inherent His101 formed a hydrogen bond with the O5 of RNS to fix the substrate for the isomerization reaction. This may explain why the enzymatic activity of H101N decreased (Supplemental Table S1), giving the two conformations of the bound substrate, a linear form and pyranose-ring form.

The α-anomer (α-RPS) was found at the sub-binding site, while the β-anomer (β-RPS) was found at the catalytic site, which is indispensable for metal-coordination by O1, O2, and O3 through the isomerization reaction. The narrow passageway from the sub-binding site to the catalytic site may fit the β-anomer, because the α-anomer with two successive axial hydroxyl groups (O1 and O2) gave a larger molecule than that of the β-anomer. The axial O1 and O2 of the α-anomer also formed hydrogen bonds with Gly63(N) and Trp57(O), respectively, anchoring a substrate at the sub-binding site. For L-rhamnopyranose, ^1H NMR in D_2O and graphitized carbon column chromatography showed 40% and 27% β-anomer in solution, respectively, and molecular mechanics calculations gave almost the same steric energies to the α-anomer (11.18 kcal/mol) and β-anomer (10.94 kcal/mol) [35], suggesting that L-rhamnopyranose exits the α-anomer and β-anomer comparably. The sub-binding site is expected to recognize the anomer's structure, allowing the β-anomer to pass into the catalytic site. We previously proposed that the C-terminal region has a role in the flip-flop movement on the inter-molecular surface of Mol-A/Mol-B or Mol-C/Mol-D, helping substrate-binding and/or

substrate-release, based on the X-ray structures and kinetic analysis of mutant *P. stutzeri* L-RhIs [17]. Various conformations of C-terminal regions were also found in this study. The tentatively bound α-anomer at the sub-binding site may possibly have been removed by the C-terminal region with dynamic motion. The substrate-binding pattern and conformation of the C-terminal region in the tetramer may indicate allosteric regulation of the enzyme, but experimental evidence for this regulation has not yet been obtained.

The bound α-APS at the catalytic site adopts the boat conformation of the pyranose-ring (Figs. 1B and 3C), the oxygen atoms of which had almost the same positions as those of β-RPS, as shown in Fig. 4. Usually, the boat conformation of the pyranose-ring is unfavorable in steric considerations. The bound α-APS forms metal-coordination with Mn1 and Mn2 and hydrophobic interactions with Trp179 and Phe66*, which stabilizes the protein–substrate complex, compensating for the high steric energy in the boat conformation. Unfortunately, the catalytic water molecule could not be found due to low resolution (2.38 Å), and the pyranose-ring opening mechanism of α-APS is still ambiguous. Binding of D-allopyranose to the sub-binding site was not found because the affinity of the sub-binding site for D-allopyranose without a hydrophobic methyl group may be lower than that for L-rhamonopyranose.

Each step of the catalytic reaction of *P. stutzeri* L-RhI could be elucidated, as shown in Fig. 5. A substrate, L-rhamnopyranose, approached the sub-binding site on the accessible surface of Mol-A/Mol-B or Mol-C/Mol-D, helped by the dynamic motion of the C-terminal region (Ala421–Ile430). The sub-binding site allowed the β-anomer (β-RPS) to pass through to the catalytic site. β-RPS formed metal-coordination with O1, O2, and O3, and a catalytic water molecule (W1) transferred a proton from O1 to O5 to open the pyranose-ring (Fig. 5A). This pyranose-ring opening mechanism is different from that of *Streptomyces olivochromogenes* D-xylose isomerase, in which His53 gives a proton to O5 (Supplemental Fig. 1B) [21]. The conformation of the linear substrate changed with rotation around C3–C4 (Fig. 5B). The hydride-shift from C2 to C1 occurred with the transfer of a proton from O2 to O1 assisted by a catalytic water molecule (W1) (Fig. 5C). After the isomerization to L-rhamnulose, O5 nucleophilly attacked C2 (carbonyl carbon) to form a hemiacetal, β-RFS, released from the catalytic site. In the reverse reaction, we proposed that Asp327 was responsible for furanose-ring opening, helping the transfer of a proton from O2 to O5 (Fig. 5D), followed by the hydride-shift from C1 to C2 (Fig. 5F and G), because bound substrates in a furanose-ring form (β-RFS) were found in D327N [16]. However, this study showed that the catalytic water molecule is also responsible for furanose-ring opening in the same manner as pyranose-ring opening. Indeed, the catalytic water molecule formed hydrogen bonds with O2 (3.1 Å) and O5 (2.8 Å) of β-RFS, likely acting as an acid/base catalyst in furanose-ring opening (Fig. 5E). In the case of the D327/β-RFS complex, the substituted Asn327(ND), which formed hydrogen bonds with the O2 and O5 of β-RFS, contributed to the steady enzyme/β-RFS complex (Fig. 3D), fixing bound substrates in a furanose-ring form.

To the best of our knowledge, the reported structural study of *P. stutzeri* L-RhI is the first example of an enzyme including substrates in pyranose ring, linear, and furanose ring forms. Each step of the catalytic reaction could be elucidated, providing insight into the relationship between the structure and function of sugar isomerase.

5. PDB accession number

Coordinates and structure factors of H101N/L-rhamnose and H101N/D-allose have been deposited in the Protein Data Bank under Accession codes 4GJI and 4GJJ, respectively.

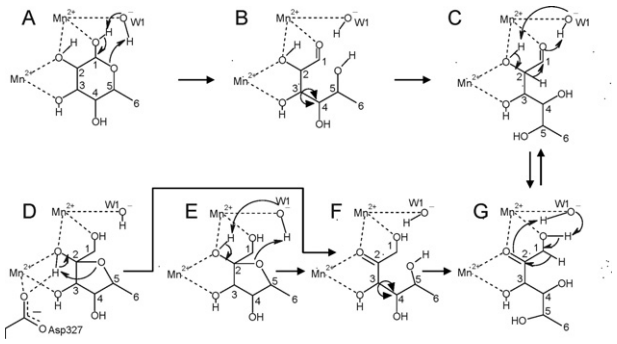

Fig. 5. Proposed catalytic reaction mechanism including sugar-ring openings of *P. stutzeri* L-RhI.

Acknowledgements

This study was supported in part by the Grant-in-Aid for Young Scientist (B) (23770122) from the Ministry of Education, Culture, Sports, Science, and Technology of Japan, and by a fund for Young Scientists 2010–11 and Characteristic Prior Research 2009–2011 from Kagawa University. This research was performed with the approval of the Photon Factory Advisory Committee and the National Laboratory for High Energy Physics (2009G512, 2010G582 and 2011G504), and the Priority Program for Disaster-Affected Quantum Beam Facilities of SPring-8 (2011GA1873), Japan.

Appendix A Supplementary material

Supplementary material associated with this article can be found, in the online version, at doi:10.1016/j.fob.2012.11.008.

References

[1] Wilson D.M., Ajl S. (1957) Metabolism of L-rhamnose by *Escherichia coli*. I. L-rhamnose isomerase. J. Bacteriol. 73, 410–414.
[2] Domagk G.F., Zech R. (1963) On the decomposition of desoxy sugars by bacterial enzymes. I. L-Rhamnose-Isomerase from *Lactobacillus plantarum*. Biochem. Z. 339, 145–153.
[3] Levinson S.L., Krulwich T.A. (1976) Metabolism of L-rhamnose in Arthrobacter pyridinolis. J. Gen. Microbiol. 96, 277–286.
[4] Al-Zarban S., Heffernan L., Nishitani J., Ransone L., Wilcox G. (1984) Positive control of the L-rhamnose genetic system in *Salmonella typhimurium* LT2. J. Bacteriol. 158, 603–608.
[5] Bhuiyan S.H., Itami Y., Izumori K. (1997) Isolation of an L-rhamnose isomerase-constitutive mutant of *Pseudomonas* sp. strain LL172: purification and characterization of the enzyme. J. Ferment. Bioeng. 84, 319–323.
[6] Leang K., Takada G., Ishimura A., Okita M., Izumori K. (2004) Cloning, nucleotide sequence, and overexpression of the L-rhamnose isomerase gene from *Pseudomonas stutzeri* in *Escherichia coli*. Appl. Environ. Microbiol. 70, 3298–3304.
[7] Leang K., Takada G., Fukai Y., Morimoto Y., Granstrom T.B., Izumori K. (2004) Novel reactions of L-rhamnose isomerase from *Pseudomonas stutzeri* and its relation with D-xylose isomerase via substrate specificity. Biochim. Biophys. Acta. 1674, 68–77.
[8] Takata G., Uechi K., Taniguchi E., Kanbara Y., Yoshihara A., Morimoto K. et al. (2011) Characterization of *Mesorhizobium loti*L-rhamnose isomerase and its application to L-talose production. Biosci. Biotechnol. Biochem. 75, 1006–1009.
[9] Poonperm W., Takata G., Okada H., Morimoto K., Granström T.B., Izumori K. (2007) Cloning, sequencing, overexpression and characterization of L-rhamnose isomerase from *Bacillus pallidus* Y25 for rare sugar production. Appl. Microbiol. Biotechnol. 76, 1297–1307.
[10] Prabhu P., Doan T.T., Jeya M., Kang L.W., Lee J.K. (2011) Cloning and characterization of a rhamnose isomerase from *Bacillus halodurans*. Appl. Microbiol. Biotechnol. 89, 635–644.
[11] Park C.S., Yeom S.J., Lim Y.R., Kim Y.S., Oh D.K. (2010) Characterization of a recombinant thermostable L-rhamnose isomerase from Thermotoga maritima ATCC 43589 and its application in the production of L-lyxose and L-mannose. Biotechnol. Lett. 32, 1947–1953.
[12] Lin C.J., Tseng W.C., Lin T.H., Liu S.M., Tzou W.S., Fang T.Y. (2010) Characterization of a thermophilic L-rhamnose isomerase from Thermoanaerobacterium saccharolyticum NTOU1. J. Agric. Food Chem. 58, 10431–10436.

[13] Lin C.J., Tseng W.C., Fang T.Y. (2011) Characterization of a thermophilic L-rhamnose isomerase from *Caldicellulosiruptor saccharolyticus* ATCC 43494. J. Agric. Food Chem. 59, 8702–8708.
[14] Korndörfer I.P., Fessner W.D., Matthews B.W. (2000) The structure of rhamnose isomerase from *Escherichia coli* and its relation with xylose isomerase illustrates a change between inter and intra-subunit complementation during evolution. J. Mol. Biol. 300, 917–933.
[15] Yoshida H., Yamada M., Ohyama Y., Takada G., Izumori K., Kamitori S. (2007) The structures of L-rhamnose isomerase from *Pseudomonas stutzeri* in complexes with L-rhamnose and D-allose provide insights into broad substrate specificity. J. Mol. Biol. 365, 1505–1516.
[16] Yoshida H., Yamaji M., Ishii T., Izumori K., Kamitori S. (2010) Catalytic reaction mechanism of *Pseudomonas stutzeri*L-rhamnose isomerase deduced from X-ray structures. FEBS J. 277, 1045–1057.
[17] Yoshida H., Takeda K., Izumori K., Kamitori S. (2010) Elucidation of the role of Ser329 and the C-terminal region in the catalytic activity of *Pseudomonas stutzeri*L-rhamnose isomerase. Protein Eng. Des. Sel. 23, 919–927.
[18] Rose I.A. (1975) Mechanism of the aldose–ketose isomerase reactions. Adv. Enzymol. Relat. Areas Mol. Biol. 43, 491–517.
[19] Carrell H.L., Glusker J.P., Burger V., Manfre F., Tritsch D., Biellmann J.F. (1989) X-ray analysis of D-xylose isomerase at 1.9 Å: native enzyme in complex with substrate and with a mechanism-designed inactivator. Proc. Natl. Acad. Sci. USA. 86, 4440–4444.
[20] Farber G.K., Glasfeld A., Tiraby G., Ringe D., Petsko G.A. (1989) Crystallographic studies of the mechanism of xylose isomerase. Biochemistry. 28, 7289–7297.
[21] Fenn T.D., Ringe D., Petsko G.A. (2004) Xylose isomerase in substrate and inhibitor Michaelis states: atomic resolution studies of a metal-mediated hydride shift. Biochemistry. 43, 6464–6474.
[22] Kovalevsky A.Y., Katz A.K., Carrell H.L., Hanson L., Mustyakimov M., Fisher S.Z. et al. (2008) Hydrogen location in stages of an enzyme-catalyzed reaction: time-of-flight neutron structure of D-xylose isomerase with bound D-xylulose. Biochemistry. 47, 7595–7597.
[23] Otwinowski, Z., Minor, W. (1997) Processing of X-ray diffraction data collected in oscillation mode in: Methods in Enzymology: Macromolecular Crystallography, Part A, Vol. 276, pp. 307–326.
[24] Collaborative Computational Project 4. (1994) The CCP4 suite: programs for protein crystallography. Acta Crystallogr. Sect. D 50, 760–763.
[25] Vagin A., Teplyakov A. (1997) MOLREP: an automated program for molecular replacement. J. Appl. Cryst. 30, 1022–1025.
[26] Emsley P., Cowtan K. (2004) Coot: model-building tools for molecular graphics. Acta Crystallogr. Sect. D. 60, 2126–2132.
[27] McRee D.E. (1999) XtalView/Xfit: a versatile program for manipulating atomic coordinate and electron density. J. Struct. Biol. 125, 156–165.
[28] McRee D.E. (1993) XtalView: In Practical Protein Crystallography. Academic Press. Inc.
[29] Murshudov G.N., Vagin A.A., Dodson E.J. (1997) Refinement of macromolecular structures by the maximum-likelihood method. Acta Crystallogr. Sect. D. 53, 240–255.
[30] Brunger A.T. (1993) X-PLOR 3.1: A System for X-ray Crystallography and NMR. New Haven and London: Yale University Press.
[31] Ramachandran G.N., Sasisekharan V. (1968) Conformation of polypeptides and protein. Adv. Protein Chem. 23, 283–437.
[32] Laskowski R.A., MacArthur M.W., Moss D.S., Thornton J.M. (1992) PROCHECK v.2: Programs to Check the Stereochemical Quality of Protein Structures. Oxford, England: Oxford Molecular Ltd.
[33] DeLano W.L. (2002) The PyMOL Molecular Graphics System. San Carlos, CA, USA: DeLano Scientific; http://www.pymol.org.
[34] Dishe Z., Borenfreud E. (1951) A new spectrophotometric method for the detection of keto sugars and trioses. J. Biol. Chem. 192, 583–587.
[35] Rockey W.M., Dowd M.K., Reilly P.J., French A.D. (2001) Modeling of deoxyaldohexopyranosyl ring puckering with MM3(92). Carbohydr. Res. 335, 261–273.